HHS Public Access

Author manuscript

Cancer Res. Author manuscript; available in PMC 2016 May 01.

Published in final edited form as:

Cancer Res. 2015 May 1; 75(9): 1846–1858. doi:10.1158/0008-5472.CAN-14-2718.

Aberrant expression of proPTPRN2 in cancer cells confers resistance to apoptosis

Alexey V. Sorokin[1], **Binoj C. Nair**[1], **Yongkun Wei**[2], **Kathryn E. Aziz**[1], **Valentina Evdokimova**[4], **Mien-Chie Hung**[2,3], and **Junjie Chen**[1,*]

[1]Department of Experimental Radiation Oncology, The University of Texas MD Anderson Cancer Center, Houston, Texas, 77030, USA

[2]Department of Molecular and Cellular Oncology, The University of Texas MD Anderson Cancer Center, Houston, Texas, 77030, USA

[3]Center for Molecular Medicine and Graduate Institute of Cancer Biology, China Medical University, Taichung 404, Taiwan

[4]Department of Genomics, Ontario Institute for Cancer Research, Toronto, Ontario, Canada

Abstract

The protein tyrosine phosphatase receptor PTPRN2 is expressed predominantly in endocrine and neuronal cells where it functions in exocytosis. We found that its immature isoform proPTPRN2 is overexpressed in various cancers including breast cancer. High proPTPRN2 expression was associated strongly with lymph node-positive breast cancer and poor clinical outcome. Loss of proPTPRN2 in breast cancer cells promoted apoptosis and blocked tumor formation in mice, while enforced expression of proPTPRN2 in non-transformed human mammary epithelial cells exerted a converse effect. Mechanistic investigations suggested that ProPTPRN2 elicited these effects through direct interaction with TRAF2, a hub scaffold protein for multiple kinase cascades including ones that activate NF-kB. Overall our results suggest PTPRN2 as a novel candidate biomarker and therapeutic target in breast cancer.

Keywords

ProPTPRN2; TRAF2; apoptosis; breast cancer

INTRODUCTION

Reversible protein tyrosine phosphorylation is an integral part of cellular signaling which controls many if not all aspects of cell biology and development. Net protein tyrosine phosphorylation is governed by the dynamic equilibrium between two counteracting enzyme families, namely protein tyrosine kinases (PTKs) and protein tyrosine phosphatases (PTPs).

*To whom correspondence should be addressed: jchen8@mdanderson.org, Junjie Chen, Ph.D., The University of Texas MD Anderson Cancer Center, 1515 Holcombe Blvd, Houston, TX 77030, Unit Number: 066, Room Number: Y3.6006, Tel: 1-713-792-4863; Fax: 1-713-794-5369.

Conflict of interests: The authors declare no conflict of interest.

Because tyrosine kinases were mostly described as oncogenes, PTPs were initially postulated to function as tumor suppressors. However, among 37 PTPs implicated in human cancer (1, 2), approximately equal proportions have been ascribed with oncogenic and tumor suppressor activities (3). In addition to protein substrates, some PTPs were shown to dephosphorylate mRNAs, inositol phospholipids or to be catalytically inactive while remaining functional (4). The precise impact of these and other individual PTPs on tumorigenesis remain unclear.

In order to find novel cancer-associated PTPs, we interrogated publicly available databases and identified a tyrosine phosphatase-like protein PTPRN2 as being significantly overexpressed in a subset of tumors, including colon, prostate, pancreas, and breast cancers. PTPRN2, also known as phogrin, IA-2β, ICAAR and NE-6, belongs to the PTP receptor type N family. It is normally expressed in nervous system and pancreatic endocrine cells, where it exists as a mature isoform and participates in exocytosis of insulin-containing secretory granules (5). While lacking protein phosphatase activity due to two critical amino acid substitutions in its PTP domain (6), PTPRN2 possesses weak phosphatidylinositol phosphatase (PIP) activity (7). By analyzing tissue microarrays (TMAs), we found that the expression of the immature isoform, proPTPRN2, was strongly associated with lymph node-positive breast cancer and poor clinical outcome. Furthermore, we established that it is the immature proPTPRN2 but not the mature isoform that is capable of disrupting normal mammary morphogenesis and promoting tumor growth in mouse xenografts and breast cancer cell lines. Mechanistically, proPTPRN2 appears to mediate this effect through the interaction with the tumor necrosis factor receptor (TNFR)–associated factor 2 (TRAF2), by suppressing apoptosis in a TRAF2-dependent manner. Given that proPTPRN2 is expressed exclusively in cancer cells, our data provide a novel diagnostic tool and a unique targeting opportunity for treatment of aggressive lymph node-positive breast cancer.

MATHERIAL AND METHODS

Antibodies

Cleaved caspase 3, JNK1, phospho JNK1 (Thr183/Tyr185), IKKα, phospho IKKα/β (Ser176/180), IKKε, phospho IKKε (Ser172), IκB, NFκB, PKC phospho substrate, Akt, phospho Akt (Ser473), PKCα, PKCζ, phospho PKC pan (βII Ser660), TNFR1, TNFR2, Fas, DR3, DR5, TRAF2, TRADD, FADD and mouse anti-rabbit IgG (conformation specific) antibodies were obtained from Cell Signaling Technology. PTPRN2 (HPA026656, SAB4502542 and HPA006900), FLAG(M2), HA, β-actin, MEMO1, PARP1 monoclonal (C-2-10), and α-tubulin monoclonal antibodies were obtained from Sigma. Ki-67 antibody was obtained from Abcam. c-Myc antibody was obtained from Santa Cruz Biotechnology. μ-calpain antibody was obtained from EMD Millipore. Sintaxin 6, Calnexin and E cadherin antibodies were obtained from BD Biosciences. Phospho TRAF2 (Ser11) antibody was kindly provided by Dr. Hasem Habelhah at the University of Iowa (USA).

Plasmids

All constructs were generated by polymerase chain reaction and subcloned into pDONR201 vector using Gateway technology (Invitrogen). The entry clones with corresponding cDNAs

were transferred into Gateway-compatible destination vectors with an N-terminal Myc epitope or a C-terminal SFB tag, or into a doxycycline-inducible vector with a C-terminal SFB tag. All constructs were verified by sequencing. GFP-FLuc-Lentiviral vector was described previously (8).

Tandem affinity purification of SFB-tagged protein complexes

HEK293T cells were transfected with plasmids encoding SFB-tagged proteins. Cell lines stably expressing the tagged protein were selected by culturing in medium containing puromycin (2 μg/ml) and confirmed by immunofluorescence staining and Western blot analysis. Tandem affinity purification was performed as described previously (9). The eluted proteins were identified by mass spectrometry analysis, which was performed by the Taplin Biological Mass Spectrometry Facility (Harvard Medical School).

Cell culture and transfection

HEK293T, HeLa, MCF7, MCF10A, SKBR3, MDA-MB-231, MDA-MB-468, MDA-MB-435, MDA-MD-436, MDA-MB-453, T47D, BT474, AU565, A498, ACHN, 769-P, 486-O, VCap, PC3, BPH1, DU145, RKO, HCT116, HCT15, 639V, 647V, HT1197, HT1376, RT4, and T24 cells were purchased from American Type Culture Collection (ATCC) and cultured under conditions specified by the manufacturer. MCF10A cells were maintained as described previously (10). Cells were tested for mycoplasma contamination. Cell transfection was performed using Lipofectamine 2000 or polyethyleneimine, according to the manufacturer's protocols.

Flow cytometry, cell growth and viability assays

To determine growth rates, equal numbers of cells were plated onto 6-cm dishes. Beginning the next day, cells were trypsinized and counted daily. To determine cell viability, cells were trypsinized and diluted with 0.4% trypan blue. Flow cytometry was performed as described previously (11). Briefly, cells were fixed in 70% (v/v) cold ethanol and stained with 20 μg/ml propidium iodide (Sigma) and 20 μg/ml DNase free RNase in phosphate-buffered saline at room temperature in the dark for 30 minutes and analyzed using a BD Accuri C6 flow cytometer (BD Biosciences).

Virus packaging and infection

pLKO.1 PTPRN2 shRNA (TRCN0000003247 [#1], TRCN0000003248 [#2], TRCN0000003249 [#3], TRCN0000003250 [#4], TRCN0000003251 [#5]) and pLKO.1 TRAF2 shRNA (TRCN0000367433 [#1], TRCN0000367467 [#2], TRCN0000004571 [#3]) sets were purchased from Sigma. Lentiviral packaging plasmids (pMD2.G and psPAX2) were kindly provided by Dr. Songyang. The production of lentiviruses and infection of target cells was performed as described previously (9).

3D Matrigel and soft agar assays

The 3D Matrigel assay was performed as described previously (10, 12). Cells (2.5×10^3) were added to 1.5 ml of growth medium with 0.2% agar (in the presence or absence of 1 μg/ml doxycycline) and layered onto 2 ml of 0.5% agar beds in 6-well plates. Cells were fed

with 1 ml of medium every 3 days for 30 days, and colonies were then examined by phase-contrast microscopy and photographed. Colonies larger than 30 μm in diameter were considered positive.

Western blot analysis and immunofluorescence microscopy

Western blot analysis was performed as described previously (13, 14). For immunofluorescence microscopy, cells cultured on coverslips were washed with phosphate-buffered saline, fixed with 3% paraformaldehyde for 20 minutes, and permeabilized with 0.5% (v/v) Triton X-100 solution for 5 minutes. Coverslips were washed with PBS and immunostained with primary antibodies in 5% goat serum for 60 minutes. Cells were then washed and incubated with rhodamine- or FITC-conjugated secondary antibodies for 60 minutes, and nuclei were stained with 1 μg/ml 4′,6-diamidino-2-phenylindole (DAPI). Slides were mounted and visualized using a Nikon ECLIPSE E800 fluorescence microscope with a Nikon Plan Fluor 10× objective lens at room temperature. Cells were photographed using a SPOT camera (Diagnostic Instruments) and analyzed using Photoshop software (Adobe).

Tumor xenograft studies and bioluminescence imaging

All animal experiments were performed in accordance with a protocol approved by the Institutional Animal Care and Use Committee of The University of Texas MD Anderson Cancer Center. For xenograft tumor assays, 5×10^6 tumor cells were resuspended in 100 μl of Matrigel diluted with PBS at 1:1 ratio and injected subcutaneously into flanks of anesthetized 6- to 8-week-old female BALB/c mice. Orthotopic tumors were developed by injecting 1×10^6 cells in 100 μl of PBS into mammary fat pads. Mice were sacrificed when they met the institutional criteria for tumor size and overall health condition. The tumors were removed and measured. For bioluminescence imaging, 150 mg/kg body weight D-Luciferin (Firefly, potassium salt, PerkinElmer) was injected intra-peritoneally 15 min before imaging. During imaging, anesthesia was maintained by nose delivery of isoflurane. Images were acquired with the Xenogen IVIS Lumina and analyzed with the Living Image software package (Version: 4.3.1.0.15766, Xenogen Corp.).

IHC analysis of TMA slides

All TMAs were purchased from US Biomax or the NCI Cancer Diagnosis Program (NCI CDP). TMAs from US Biomax (BC081120) contain 100 cases of invasive breast carcinoma and 10 specimens of cancer-adjacent normal breast tissue. The NCI CDP Progression TMAs consist of 3 different case sets, including 242 analyzable cases of invasive breast carcinoma and 29 analyzable cases of DCIS. The NCI CDP Prognostic TMAs consist of 5 nonoverlapping stage I case sets (590 specimens), 4 stage II case sets (398 specimens), and 2 stage III case sets (181 specimens).

Samples were deparaffinized and rehydrated. Antigen retrieval was done using 0.01M sodium citrate buffer (pH 6.0) in a microwave oven. To block endogenous peroxidase activity, the sections were treated with 1% hydrogen peroxide in methanol for 30 minutes. After 1 hour of preincubation in 10% normal serum to prevent nonspecific staining, the samples were incubated with anti-proPTPRN2 (HPA026656; 1:200) or cleaved caspase 3 antibody (1:200) at 4°C overnight. The sections were then treated with a biotinylated

secondary antibody (Vector Laboratories, PK-6101, 1:200) and incubated with avidin-biotin peroxidase complex solution (1:100) for 1 hour at room temperature. Color was developed with the 3-amino-9-ethylcarbazole solution. Counterstaining was carried out using Mayer's hematoxylin. H-score system was used to quantify IHC results. For proPTPRN2 staining: 0 < low ≤ 75, 75 < high ≤ 300; for cleaved caspase 3 staining: 0 < low ≤ 6, 6 < high ≤ 300.

All immunostained slides were scanned on the Automated Cellular Image System III (Dako, Denmark) for quantification by digital image analysis. A total score of protein expression was calculated from both the percentage of immunopositive cells and the immunostaining intensity. High and low protein expression was defined using the mean score of all samples as a cutoff point. Negative expression indicated no detectable immunoreactivity. Spearman rank correlation was used for statistical analysis of the correlation between proPTPRN2 and the clinical parameters. Kaplan-Meier survival analysis and the log-rank test were used for statistical analysis of the correlation between proPTPRN2 and clinical survival outcomes.

RESULTS

ProPTPRN2 is overexpressed in breast tumors and predicts poor clinical outcome

Given an essential role of tyrosine phosphorylation in tumorigenesis, we set out to identify novel protein tyrosine phosphatases whose expression is associated with carcinogenesis and which may thus represent druggable targets. Search of publicly available databases revealed that a tyrosine phosphatase-like gene *PTPRN2* was overexpressed in various cancers, including T-cell lymphoma, lung, prostate, skin, renal and breast cancer at both mRNA and protein levels (Supplementary Fig. 1). In particular, based on the Cancer Genome Atlas (TCGA) datasets *PTPRN2* mRNA level was increased in breast cancers by 2–4 fold (Supplementary Fig. 1D). Of further note, the *PTPRN2* gene copy number was not significantly altered in most cancers (Supplementary Fig. 1C), suggesting epigenetic mechanisms of its activation, in agreement with a recent study (15).

Interestingly, according to Protein Atlas database, 4 of 12 breast tumors (33%) were positive for the immature proPTPRN2 isoform (Supplementary Fig. 1F), which is known to be synthesized on the endoplasmic reticulum and has to undergo N-glycosylation and cleavage to generate mature isoforms of approximately 60–70 kDa (16, 17). By Western blot analysis using antibodies capable of recognizing both isoforms (Fig. 1A and Supplementary Fig. 2), we confirmed proPTPRN2 protein expression in various breast, renal, prostate and colorectal cancer cell lines, while no mature ~60 kDa isoform was detected (Fig. 1B). Furthermore, in a panel of breast cancer cell lines representing luminal and basal subtypes, we detected exclusively the ~100–120 kDa pro-isoform of PTPRN2 using two different antibodies specifically raised against the pro-region of the protein, along with those recognizing both isoforms (Fig. 1A and Supplementary Fig. 2). Based on these observations, we conclude that proPTPRN2 is not converted into mature isoform, probably due to lack of natural processing mechanism in these cells. Importantly, proPTPRN2 was not observed in non-transformed MCF10A mammary epithelial cells and its expression was somewhat higher in luminal estrogen receptor-positive cell lines compared to basal subtypes (Fig. 1C), although more cell lines need to be analyzed for a definite conclusion. Overall, these data

indicate that pro-isoform of PTPRN2 is widely expressed in cancer cells of different origin, including breast which has been studied here in more detail.

In agreement with Western blotting results, proPTPRN2 expression was also detected by immunohistochemistry, using commercially available breast cancer TMAs. Of the 10 normal breast tissue samples we examined, none showed detectable levels of proPTPRN2 (Fig. 1D). In contrast, 45 out of 99 invasive breast carcinoma specimens (45%) displayed positivity for proPTPRN2 (Fig. 1D), revealing significant correlation with invasive breast carcinoma compared to normal mammary tissue ($P = 0.005$).

Using the National Cancer Institute (NCI) Progression TMAs, we found no significant differences in proPTPRN2 expression between ductal carcinoma *in situ* (DCIS) and invasive breast carcinoma specimens, with 12 out of 29 DCIS samples (41.4%) and 92 of 212 invasive breast carcinoma samples (43.4%) showing proPTPRN2 positivity (Fig. 1E). Consistent with Western blotting results (Fig. 1C), we observed a modest increase in proPTPRN2 staining intensity in estrogen and progesterone receptor-positive tumors ($P = 0.230$ and $P = 0.077$, accordingly) (Fig. 1F). Similar correlation between proPTPRN2 and estrogen receptor status was also observed in the TCGA database (Supplementary Fig. 1D). Of further note, although proPTPRN2 expression was not significantly associated with a particular tumor stage ($P = 0.089$), it was modestly elevated at T1 stage compared to T2 (Fig. 1F), suggesting that proPTPRN2 expression may play a role at earliest stages of tumorigenesis.

To determine whether proPTPRN2 expression has a prognostic significance, we utilized NCI Prognostic TMAs containing 1,169 breast tumor specimens with a long-term clinical follow-up record. Subsequent Kaplan-Meier analysis revealed that patients with lymph node-positive breast cancer with high proPTPRN2 levels displayed significantly poorer overall survival ($P = 0.009$), recurrence-free survival ($P = 0.018$) and distant metastasis-free survival ($P = 0.008$) than those with low proPTPRN2 levels (Fig. 1G). Therefore, high proPTPRN2 expression has a potential to be used as a clinical marker associated with aggressiveness and disease progression in breast cancer patients.

Reduced proPTPRN2 expression is associated with impaired proliferation and increased apoptosis in breast cancer cells and clinical samples

Although the involvement of mature PTPRN2 in insulin secretion by pancreatic beta-cells and its association with insulin-dependent diabetes mellitus are well established (5), the role of the mature or pro-isoforms in tumorigenesis has never been elucidated. To study how ablation of proPTPRN2 expression may affect cell growth, we used two highly proliferative and aggressive breast cancer cell lines, MDA-MB-468 and SKBR3, as a model for this study. Downregulation of proPTPRN2 expression in these cell lines by stable expression of specific targeting shRNAs resulted in a significant reduction of their growth kinetics, while not affecting PTPRN2-negative MCF10A cells (Fig. 2A and B). Moreover, when subcutaneously implanted into mouse flanks, these cells failed to form palpable tumors, as measured by tumor size (Fig. 2C) and luminescence (Fig. 2D and E). These results indicate that proPTPRN2 is required for tumor growth.

Further analysis of the cell cycle distribution of PTPRN2 knockdown cells revealed that a significant proportion of these cells accumulated in sub-G1, and this phenotype was partially rescued by a general caspase inhibitor Z-VAD-FMK but not a necrosis inhibitor necrostatin-1 (Fig. 3A). Enhanced apoptosis in PTPRN2 knockdown cells was further confirmed by detection of cleaved caspase 3 and cleaved PARP1 (Fig. 3B), and is in agreement with previous studies showing that knockdown of PTPRN2 induced apoptosis in large-scale siRNA and shRNA library screenings (18, 19). Most importantly, expression of shRNA-resistant proPTPRN2 fused with the C-terminal triple-epitope (SFB, S protein, Flag, and streptavidin-binding peptide) rescued cell death caused by PTPRN2 shRNA, as shown by reduction in the sub-G1 population from 32% in PTPRN2 knockdown cells to 13% in those expressing the resistant form (Fig. 3C and D). Also, expression of shRNA-resistant proPTPRN2-SFB but not that of mature PTPRN2 restored the ability of PTPRN2 knockdown cells to form tumors in mice (Fig. 3E). Together, these results indicate that proPTPRN2 has a unique function in promoting tumor growth and survival both *in vitro* and *in vivo*.

IHC analysis of breast cancer specimens revealed an inverse correlation between overall proPTPRN2 and cleaved caspase 3 staining (Pearson $r = -0.236$, $P < 0.0001$; Fig. 3F). Moreover, within the cohort with high levels of cleaved caspase 3 ($6 <$ high ≤ 300, H-score system), 100 of 111 samples (90.1%) showed no proPTPRN2 expression (Fig. 3G, case B). Similarly, within the cohorts with high levels of proPTPRN2 ($75 <$ high ≤ 300, H-score system), 40 of 51 samples (78.4%) showed no cleaved caspase 3 staining (Fig. 3G, case A), suggesting a correlation between proPTPRN2 expression and block of apoptosis in human tumors.

ProPTPRN2 expression increases acinar size and promotes tumor growth

To further investigate the role of proPTPRN2 in breast cancer etiology, we generated MCF10A cells stably expressing proPTPRN2 alone or together with the known oncogenic protein ErbB2/HER2; both proteins were SFB-tagged and doxycycline-inducible (Fig. 4A). Expression of proPTPRN2 did not cause any morphological changes in monolayer culture (data not shown), nor did it provide any growth advantage for the exponentially growing monolayer cells (Fig. 4B), or colony formation/anchorage-independent growth in soft agar (Fig. 4C), properties that are frequently associated with tumorigenic transformation. Therefore, proPTPRN2 by itself is unable to induce neoplastic transformation.

However, expression of proPTPRN2, but not mature PTPRN2, in MCF10A cells did increase acinar size (Fig. 4D and Supplementary Fig. 3). ProPTPRN2 expressing cells formed significantly larger colonies, with or without HER2 co-expression (Fig. 4E). Normally, MCF10A cells form polarized acinar structures with hollow lumen in Matrigel at day 10+, when inner cells die via apoptosis (10). Using laminin V and Ki67 as markers for basal polarity and proliferation, respectively, we found that although apical-basal polarity was not affected in proPTPRN2 expressing cells, acini lumen was not formed and was filled with proliferating cells (Fig. 4F and G). These data suggest that proPTPRN2 may block apoptosis and therefore disrupt normal mammary morphogenesis.

In agreement with the aforementioned results, MDA-MB-231 cells engineered to express proPTPRN2 formed significantly larger tumors in mouse xenografts compared to vector alone cells (Fig. 4H). Remarkably, this effect was observed only with proPTPRN2 and not with the mature form (Fig. 4H), indicating that proPTPRN2 has a unique function in promoting tumor growth and survival.

ProPTPRN2 but not the mature PTPRN2 isoform forms a complex with TRAF2

Search for potential mediators of proPTPRN2 effects revealed a multiple components of IκB/NF-κB and c-Jun N-terminal kinase (JNK)/AP-1 signaling pathways as being affected by proPTPRN2 downregulation (Supplementary Fig. 4). Since both these pathways are controlled by the action of a RING domain E3 ubiquitin ligase called TRAF2 which promotes Lys63-linked ubiquitination of various components involved in NF-kB and JNK signaling or serves as an adaptor protein (20, 21), we speculated that proPTPRN2 may interact with or regulate one of the components of the TRAF2 complex. Indeed, using a panel of breast cancer cell lines we found a correlation between proPTPRN2 and the expression levels of the major component of the TRAF2 complex TRAF2 and TRADD, while death receptors such as TNFR1, TNFR2, FasR, DR3, DR5 and an adaptor protein FADD were not affected (Fig. 5A). Furthermore, mass-spectrometry of proteins interacting with proPTPRN2-SFB revealed several other components of the TRAF2 complex, including members of the inhibitors of apoptosis (IAP) family such as XIAP, cIAP1, cIAP2 (Fig. 5B). Association of these proteins with proPTPRN2 in the TRAF2 complex was confirmed by co-immunoprecipitation after their co-expression in HEK293T cells, with TRAF2 showing a stronger binding than the others (Fig. 5C).

To map the proPTPRN2 binding site on TRAF2, we generated a set of truncated TRAF2 mutants lacking several domains essential for its activity (Fig. 5D and E). Co-expression of the corresponding mutants with proPTPRN2-SFB in HEK293T cells followed by co-immunoprecipitation revealed that deletion of the N-terminal part of TRAF2 (1–33 residues; D1 mutant) dramatically reduced its interaction with proPTPRN2 (Fig. 5E). This region, together with the adjacent RING-type Zn-finger and 2 TRAF2-type Zn-finger domains, is required for Lys63-linked autoubiquitination and activation of downstream signaling events (22). Notably, deletion of the two C-terminal subdomains (coiled coil [Cc] and MATH) responsible for self-association and interactions with death receptors and other proteins did not affect TRAF2 binding to proPTPRN2 (Fig. 5E). These results suggest that proPTPRN2 may regulate TRAF2 autoubiquitination and activation via direct binding to its 33 N-terminal amino acids.

We next sought to determine whether mature PTPRN2 or the proPTPRN2 lacking the PTP domain (Fig. 5F) are capable of interacting with TRAF2. We found that mature PTPRN2 did not co-immunoprecipitate with TRAF2 (Fig. 5G), indicating that the pro-region of PTPRN2 is an absolute requirement for the interaction with TRAF2. Deletion of the PTP domain reduced but did not abolish their interaction (Fig. 5G), suggesting that the PTP domain may somehow enhance or stabilize the proPTPRN2-TRAF2 complex. These results were also supported by mass-spectrometry data showing that in contrast to mature PTPRN2, the PTP deletion mutant was still able to bind to TRAF2, XIAP and cIAP1 (Fig. 5H). Interestingly

however that PTPRN2 ΔPTP failed to bind to a subset of cell surface proteins (shown in green in Fig. 5H), which may be required for PTPRN2 recruitment to plasma membrane and, therefore, for its compartmentalization with TRAF2, providing a potential explanation for the observed reduction in its binding to TRAF2 in co-immunoprecipitation experiments. Overall, these results demonstrate that only proPTPRN2 and not the mature form is capable of binding to TRAF2 via its pro-region and that the 33 N-terminal TRAF2 amino acids are required for their interaction.

ProPTPRN2 suppresses cell density-dependent apoptosis

Apoptosis can be induced by a wide range of stimuli, including high cell density (23, 24). Indeed, using MCF10A cells as a model, we found that long-term cultivation (5+ days) of MCF10A confluent monolayer culture spontaneously triggered apoptosis, as detected by cleaved caspase 3 immunofluorescence staining (Fig. 6A). This density-induced apoptosis was rescued by proPTPRN2 expression but not by mature PTPRN2 (Fig. 6A). In a complementary experiment, depletion of proPTPRN2 sensitized MDA-MB-468 cells to contact inhibition and confluence-induced apoptosis (Supplementary Fig. 5). Using series of proPTPRN2 mutants we found that neither restored protein tyrosine phosphatase activity of proPTPRN2 (+PTP), nor intrinsic phosphoinositide phosphatase activity (PIP), nor deletion of the whole 245 amino acid PTP domain affected the ability of proPTPRN2 to block apoptosis (as measured by caspase 3 cleavage) in overconfluent MCF10A cells (Fig. 6B), suggesting that only pro-region is indispensable for proPTPRN2 anti-apoptotic activity.

We also found that density-induced apoptosis was TRAF2-dependent as it was abolished by TRAF2-targeting shRNAs (Fig. 6C). In contrast to the mature form which was not capable of binding to TRAF2, association of TRAF2 with proPTPRN2 was gradually increasing with cell growth, reaching the highest levels in confluent cells (Fig. 6D and F). Similarly to the wild type, proPTPRN2 mutant proteins (−PIP) and (+PTP) but not the PTP domain deletion mutant interacted with TRAF2 in a confluence-dependent manner (Fig. 6E). These data suggest a possibility that aberrant expression of proPTPRN2 may interfere with normal functions of TRAF2, particularly those associated with regulation of cell contact-dependent growth inhibition and apoptosis.

Binding of proPTPRN2 suppresses TRAF2 phosphorylation by PKC and its complex formation with FADD

Given a possibility that proPTPRN2 specifically interferes with TRAF2 functions and that the interaction between these two drastically increased in overconfluent MCF10A cells, we investigated signaling pathways regulating confluence-dependent activation of TRAF2. TRAF2-mediated signaling is known to be regulated at multiple levels via its phosphorylation by Akt, IKKε and PKC (22, 25–28). We thus analyzed activation/phosphorylation status of Akt, IKKε and PKC using the corresponding phospho-specific antibodies. We found that since Akt phosphorylation was reduced with confluence and was not affected by TRAF2 expression (Fig. 7A), PI3K-Akt signaling is not likely to be involved in confluence-dependent TRAF phosphorylation (Fig. 7B). By contrast, IKKε phosphorylation was strongly induced in overconfluent MCF10A cells while being abrogated by ectopic expression of TRAF2 (Fig. 7A), indicating that TRAF2 may act

upstream of IKKε. Most importantly, PKC phosphorylation was enhanced with confluence and correlated well with TRAF2 phosphorylation as detected by PKC substrate phospho-specific antibody (Fig. 7A), and it also positively correlated with phosphorylation of TRAF2 at Ser-11 (Fig. 7B), one of known sites for PKC-mediated TRAF2 phosphorylation (22, 25–28). Furthermore, ectopic expression of proPTPRN2 but not the mature form drastically suppressed TRAF2 phosphorylation at Ser-11 (Fig. 7C and Supplementary Fig. 6), in agreement with our findings that the pro-region is required for TRAF2 binding (Fig. 5G). This data support the notion that proPTPRN2 interaction with TRAF2 may prevent the latter from being activated/phosphorylated by PKC in response to confluence/contact inhibition.

To establish if diminished phosphorylation of TRAF2 by PKC in proPTPRN2 expressing cells may have functional significance, confluent monolayer MCF10A cells were cultured for more than 5 days and monitored for signs of apoptosis (cleaved caspase 3) by immunofluorescence microscopy and immunoblotting. As shown in Figs. 6A and 7C, high cell density spontaneously triggered caspase 3 cleavage/apoptosis in MCF10A cells, while ectopic expression of proPTPRN2 prevented activation of apoptosis (Figs. 6A and 7C, compare lanes 3 and 4). Moreover, proPTPRN2 was capable of suppressing apoptosis caused by 12-O-Tetradecanoylphorbol-13-acetate (TPA), a PKC activator known to induce apoptosis in breast cancer cell lines (29, 30). This was also accompanied by diminished TRAF2 phosphorylation at Ser-11, in spite of high levels of phosphorylated PKC in TPA-treated cells (Fig. 7D). Therefore, proPTPRN2 blocks PKC-mediated phosphorylation of TRAF2 as well as its subsequent activation and the ability to initiate apoptotic response.

Given that FADD is one of the major effectors acting downstream of TRAF2 to initiate caspase cascades leading to apoptosis (31), we tested the effect of proPTPRN2 on the TRAF2-FADD complex formation. In agreement with previous reports (22, 25, 26, 28), we found that TRAF2 phosphorylation at Ser-11 positively correlated with the TRAF2-FADD complex formation and caspase 3 cleavage in overconfluent MCF10A cells (Fig. 7E, compare lanes 5 and 7). Remarkably however, recruitment of FADD to the complex with TRAF2 was substantially diminished in proPTPRN2-expressing MCF10A cells (Fig. 7E, compare lines 7 and 8). Taken together with the observed reduction in phosphorylation of TRAF2 at Ser-11 and in caspase 3 cleavage in these cells, these results suggest a mechanism whereby proPTPRN2 blocks apoptosis by preventing PKC-mediated TRAF2 phosphorylation/activation and its subsequent association with FADD (Fig. 7G). This was also confirmed by knocking down endogenous proPTPRN2 in MDA-MB-468 cells, which led to enhanced TRAF2-FADD complex formation (Fig. 7F) and apoptosis (Fig. 3). Together with the observed in this study widespread expression of proPTPRN2 in breast cancers, this latter result also indicate that targeting proPTPRN2 may provide very precise tool for restoring normal cellular mechanisms of contact inhibition and apoptosis.

DISCUSSION

In this study, we demonstrated that proPTPRN2 protein is frequently overexpressed in human cancers. We showed that proPTPRN2 interacts with TRAF2, suppresses apoptosis and thus promotes tumor growth and survival. Moreover, high proPTPRN2 expression was associated with poor outcome in patients with lymph node-positive breast cancer, indicating

that overexpression of proPTPRN2 is likely to have prognostic value. Most importantly, proPTPRN2 is not expressed in normal adult cells or tissues, and PTPRN2-knockout mice showed very mild glucose intolerance and impaired glucose-stimulated insulin secretion (32). Therefore, targeting of PTPRN2 should have minimal side effects while significantly inhibiting tumor growth by inducing apoptosis, making it an attractive target candidate for cancer therapy.

We found that enforced expression of proPTPRN2 disrupted mammary morphogenesis and hollow lumen formation by blocking apoptosis, and PTPRN2 acted synergistically with HER2 to promote acinar overgrowth in Matrigel and tumor growth in mouse xenografts. This may recapitulate an oncogenic function of PTPRN2 in early breast cancer lesions such as DCIS which are characterized by loss of acinar organization and filling of the luminal space (33). In agreement with this, we observed high proPTPRN2 expression in a substantial subset of DCIS samples, supporting a notion that proPTPRN2 anti-apoptotic activity may be involved in DCIS and subsequent cancer progression.

One particularly interesting observation in our study is that high cell density-induced apoptosis in non-transformed MCF10A cells was significantly suppressed by proPTPRN2 but not by the mature PTPRN2 form. We also showed that neither PTP, nor PIP enzymatic activities were involved in proPTPRN2-mediated blockade of apoptosis, and this effect was executed through the interaction between the pro-region of PTPRN2 and the N-terminal 33 amino acids of TRAF2. Anti-apoptotic activity of proPTPRN2 was also demonstrated in large-scale cohort analysis using breast cancer TMAs, where high proPTPRN2 expression inversely correlated with that of cleaved caspase 3.

Suppression of apoptosis during carcinogenesis plays a central role in the development and progression of all human cancers (34, 35). In this regard, TRAF2 and the inhibitor of apoptosis protein (IAP) family are perhaps the most important regulators of apoptosis since they are capable of regulating both the intrinsic and extrinsic pathways (36, 37). In this study, we found that aberrantly expressed proPTPRN2 binds to the TRAF2-cIAP complex. It blocks PKC-mediated TRAF2 phosphorylation and its association with pro-apoptotic adaptor protein FADD, thereby preventing the initiation of apoptosis (Fig. 7G). Of further importance, depletion of proPTPRN2 in breast cancer cells restored confluence-dependent apoptosis, suggesting that proPTPRN2 may be a novel therapeutic target for cancer treatment.

In summary, proPTPRN2 overexpression dramatically suppressed apoptosis in a density-dependent manner in monolayer cultures and during acinar lumen formation, and proPTPRN2 promoted tumor growth in xenograft studies. Moreover, high proPTPRN2 expression was associated with poor prognosis in patients with lymph node-positive breast cancer. We thus envision that therapeutic intervention targeting proPTPRN2 may improve overall survival of breast cancer patients with high proPTPRN2 expression.

Supplementary Material

Refer to Web version on PubMed Central for supplementary material.

Acknowledgments

We thank all of our colleagues in the Chen laboratory for insightful discussions. This work was supported in part by an Era of Hope Research award to JC (W81XWH-09-1-0409). JC was also a recipient of an Era of Hope Scholar award from the Department of Defense (W81XWH-05-1-0470). This work was supported in part by the National Institutes of Health/National Cancer Institute Cancer Center Support Grant (CA016672) to The University of Texas MD Anderson's Cancer Center.

References

1. Julien SG, Dube N, Hardy S, Tremblay ML. Inside the human cancer tyrosine phosphatome. Nat Rev Cancer. 2011; 11:35–49. [PubMed: 21179176]
2. Hendriks WJ, Pulido R. Protein tyrosine phosphatase variants in human hereditary disorders and disease susceptibilities. Biochim Biophys Acta. 2013; 1832:1673–96. [PubMed: 23707412]
3. Xu Y, Fisher GJ. Receptor type protein tyrosine phosphatases (RPTPs) - roles in signal transduction and human disease. J Cell Commun Signal. 2012; 6:125–38. [PubMed: 22851429]
4. Alonso A, Sasin J, Bottini N, Friedberg I, Osterman A, Godzik A, et al. Protein tyrosine phosphatases in the human genome. Cell. 2004; 117:699–711. [PubMed: 15186772]
5. Torii S. Expression and function of IA-2 family proteins, unique neuroendocrine-specific protein-tyrosine phosphatases. Endocr J. 2009; 56:639–48. [PubMed: 19550073]
6. Magistrelli G, Toma S, Isacchi A. Substitution of two variant residues in the protein tyrosine phosphatase-like PTP35/IA-2 sequence reconstitutes catalytic activity. Biochem Biophys Res Commun. 1996; 227:581–8. [PubMed: 8878556]
7. Caromile LA, Oganesian A, Coats SA, Seifert RA, Bowen-Pope DF. The neurosecretory vesicle protein phogrin functions as a phosphatidylinositol phosphatase to regulate insulin secretion. J Biol Chem. 2010; 285:10487–96. [PubMed: 20097759]
8. Zhang XH, Wang Q, Gerald W, Hudis CA, Norton L, Smid M, et al. Latent bone metastasis in breast cancer tied to Src-dependent survival signals. Cancer Cell. 2009; 16:67–78. [PubMed: 19573813]
9. Sorokin AV, Chen J. MEMO1, a new IRS1-interacting protein, induces epithelial-mesenchymal transition in mammary epithelial cells. Oncogene. 2013; 32:3130–8. [PubMed: 22824790]
10. Debnath J, Brugge JS. Modelling glandular epithelial cancers in three-dimensional cultures. Nat Rev Cancer. 2005; 5:675–88. [PubMed: 16148884]
11. Riccardi C, Nicoletti I. Analysis of apoptosis by propidium iodide staining and flow cytometry. Nat Protoc. 2006; 1:1458–61. [PubMed: 17406435]
12. Evdokimova V, Tognon C, Ng T, Ruzanov P, Melnyk N, Fink D, et al. Translational activation of snail1 and other developmentally regulated transcription factors by YB-1 promotes an epithelial-mesenchymal transition. Cancer Cell. 2009; 15:402–15. [PubMed: 19411069]
13. Evdokimova V, Ruzanov P, Anglesio MS, Sorokin AV, Ovchinnikov LP, Buckley J, et al. Akt-mediated YB-1 phosphorylation activates translation of silent mRNA species. Mol Cell Biol. 2006; 26:277–92. [PubMed: 16354698]
14. Sorokin AV, Selyutina AA, Skabkin MA, Guryanov SG, Nazimov IV, Richard C, et al. Proteasome-mediated cleavage of the Y-box-binding protein 1 is linked to DNA-damage stress response. EMBO J. 2005; 24:3602–12. [PubMed: 16193061]
15. Smyth LJ, McKay GJ, Maxwell AP, McKnight AJ. DNA hypermethylation and DNA hypomethylation is present at different loci in chronic kidney disease. Epigenetics. 2014; 9:366–76. [PubMed: 24253112]
16. Wasmeier C, Hutton JC. Molecular cloning of phogrin, a protein-tyrosine phosphatase homologue localized to insulin secretory granule membranes. J Biol Chem. 1996; 271:18161–70. [PubMed: 8663434]
17. Hermel JM, Dirkx R Jr, Solimena M. Post-translational modifications of ICA512, a receptor tyrosine phosphatase-like protein of secretory granules. Eur J Neurosci. 1999; 11:2609–20. [PubMed: 10457160]

18. Silva JM, Marran K, Parker JS, Silva J, Golding M, Schlabach MR, et al. Profiling essential genes in human mammary cells by multiplex RNAi screening. Science. 2008; 319:617–20. [PubMed: 18239125]
19. MacKeigan JP, Murphy LO, Blenis J. Sensitized RNAi screen of human kinases and phosphatases identifies new regulators of apoptosis and chemoresistance. Nat Cell Biol. 2005; 7:591–600. [PubMed: 15864305]
20. Ofengeim D, Yuan J. Regulation of RIP1 kinase signalling at the crossroads of inflammation and cell death. Nat Rev Mol Cell Biol. 2013; 14:727–36. [PubMed: 24129419]
21. Schmukle AC, Walczak H. No one can whistle a symphony alone - how different ubiquitin linkages cooperate to orchestrate NF-kappaB activity. J Cell Sci. 2012; 125:549–59. [PubMed: 22389394]
22. Li S, Wang L, Dorf ME. PKC phosphorylation of TRAF2 mediates IKKalpha/beta recruitment and K63-linked polyubiquitination. Mol Cell. 2009; 33:30–42. [PubMed: 19150425]
23. Kuhn K, Hashimoto S, Lotz M. Cell density modulates apoptosis in human articular chondrocytes. J Cell Physiol. 1999; 180:439–47. [PubMed: 10430184]
24. Elmore S. Apoptosis: a review of programmed cell death. Toxicol Pathol. 2007; 35:495–516. [PubMed: 17562483]
25. Blackwell K, Zhang L, Thomas GS, Sun S, Nakano H, Habelhah H. TRAF2 phosphorylation modulates tumor necrosis factor alpha-induced gene expression and cell resistance to apoptosis. Mol Cell Biol. 2009; 29:303–14. [PubMed: 18981220]
26. Thomas GS, Zhang L, Blackwell K, Habelhah H. Phosphorylation of TRAF2 within its RING domain inhibits stress-induced cell death by promoting IKK and suppressing JNK activation. Cancer Res. 2009; 69:3665–72. [PubMed: 19336568]
27. Zhang L, Blackwell K, Altaeva A, Shi Z, Habelhah H. TRAF2 phosphorylation promotes NF-kappaB-dependent gene expression and inhibits oxidative stress-induced cell death. Mol Biol Cell. 2010; 22:128–40. [PubMed: 21119000]
28. Shen RR, Zhou AY, Kim E, Lim E, Habelhah H, Hahn WC. IkappaB kinase epsilon phosphorylates TRAF2 to promote mammary epithelial cell transformation. Mol Cell Biol. 2012; 32:4756–68. [PubMed: 23007157]
29. Li Y, Bhuiyan M, Mohammad RM, Sarkar FH. Induction of apoptosis in breast cancer cells by TPA. Oncogene. 1998; 17:2915–20. [PubMed: 9879997]
30. Cataisson C, Joseloff E, Murillas R, Wang A, Atwell C, Torgerson S, et al. Activation of cutaneous protein kinase C alpha induces keratinocyte apoptosis and intraepidermal inflammation by independent signaling pathways. J Immunol. 2003; 171:2703–13. [PubMed: 12928424]
31. Cabal-Hierro L, Lazo PS. Signal transduction by tumor necrosis factor receptors. Cell Signal. 2012; 24:1297–305. [PubMed: 22374304]
32. Kubosaki A, Gross S, Miura J, Saeki K, Zhu M, Nakamura S, et al. Targeted disruption of the IA-2beta gene causes glucose intolerance and impairs insulin secretion but does not prevent the development of diabetes in NOD mice. Diabetes. 2004; 53:1684–91. [PubMed: 15220191]
33. Ross DS, Wen YH, Brogi E. Ductal carcinoma in situ: morphology-based knowledge and molecular advances. Adv Anat Pathol. 2013; 20:205–16. [PubMed: 23752083]
34. Kerr JF, Winterford CM, Harmon BV. Apoptosis. Its significance in cancer and cancer therapy. Cancer. 1994; 73:2013–26. [PubMed: 8156506]
35. Hanahan D, Weinberg RA. The hallmarks of cancer. Cell. 2000; 100:57–70. [PubMed: 10647931]
36. Deveraux QL, Reed JC. IAP family proteins--suppressors of apoptosis. Genes Dev. 1999; 13:239–52. [PubMed: 9990849]
37. Habelhah H. Emerging complexity of protein ubiquitination in the NF-kappaB pathway. Genes Cancer. 2010; 1:735–47. [PubMed: 21113390]

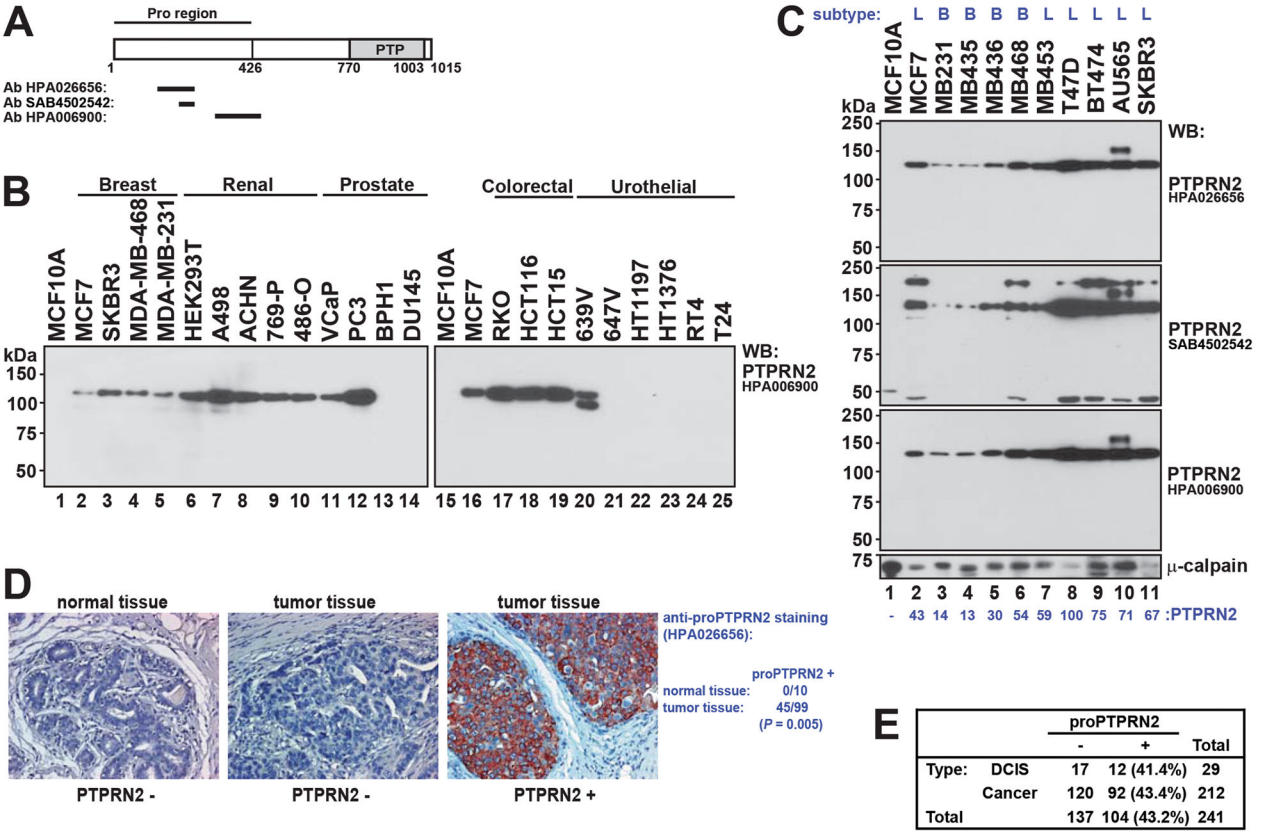

E

		proPTPRN2 -	proPTPRN2 +	Total
Type:	DCIS	17	12 (41.4%)	29
	Cancer	120	92 (43.4%)	212
Total		137	104 (43.2%)	241

F

		proPTPRN2 -	proPTPRN2 +	Total
T stage:	T1	49	44 (47.3%)	93
	T2	63	35 (35.7%)	98
	T3	3	3 (50%)	6
	T4	5	10 (66.7%)	15
Total		120	92 (43.4%)	212
N stage:	N0	45	31 (40.7%)	76
	N1-3	59	44 (44.4%)	99
M stage:	M0	82	62 (43.1%)	144
	M1	38	30 (44.1%)	68
ER status:	0	20	10 (33.3%)	30
	1	21	20 (48.8%)	41
PR status:	0	30	16 (34.8%)	46
	1	10	14 (58.3%)	24

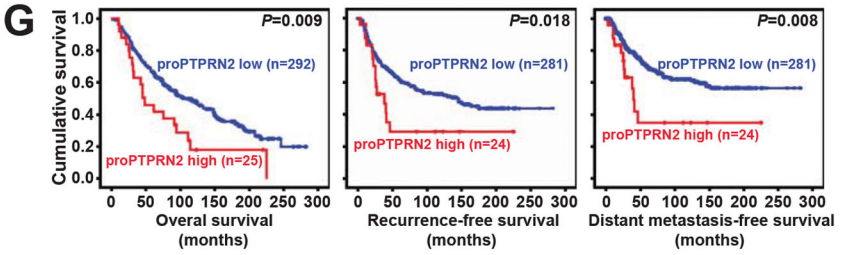

Figure 1. ProPTPRN2 is highly expressed in breast cancers and predicts poor clinical outcome

A, Domain structure of PTPRN2, isoform 1. PTP, protein-tyrosine phosphatase domain. Antibodies were raised against the indicated epitopes. B, Western blot (WB) analysis of PTPRN2 expression in human cancer cell lines using HPA006900 antibody. C, WB analysis of PTPRN2 expression in human normal breast and cancer cell lines using HPA026656, SAB4502542 and HPA006900 antibodies. μ-calpain was monitored here as a protein potentially involved in the processing of PTPRN2. Equal amounts of cell extracts were used for WB analysis. Breast cancer cell lines representing luminal (L) and basal subtypes (B) are indicated. Relative amounts of PTPRN2 from three independent experiments were indicated

at the bottom. D, ProPTPRN2 expression in normal breast tissues and invasive breast carcinomas. Representative IHC sections of 99 cases US Biomax TMAs stained with HPA026656 antibody are shown. E, ProPTPRN2 expression status in patients with invasive breast carcinoma and ductal carcinoma *in situ* (DCIS). 241 cases NCI Progression TMAs were used for IHC with HPA026656 antibody. F, The association between the absence and the presence of proPTPRN2 and clinico-pathological characteristics of tumors including TNM stage, estrogen receptor (ER) status, and progesterone receptor (PR) status. The NCI Progression TMAs were stained as in (E). G, Kaplan-Meier curves representing the probability of overall survival, recurrence-free survival (recurrence indicates tumor relapse at the primary site, the metastatic site, or both), and cumulative metastasis-free survival (free of distant metastasis) in patients with lymph node-positive breast cancer, stratified according to proPTPRN2 expression status in the primary tumor. The log-rank test *P* value reflects the significance of the correlation between proPTPRN2 positivity and poor survival outcomes, see also Supplementary Table 2.

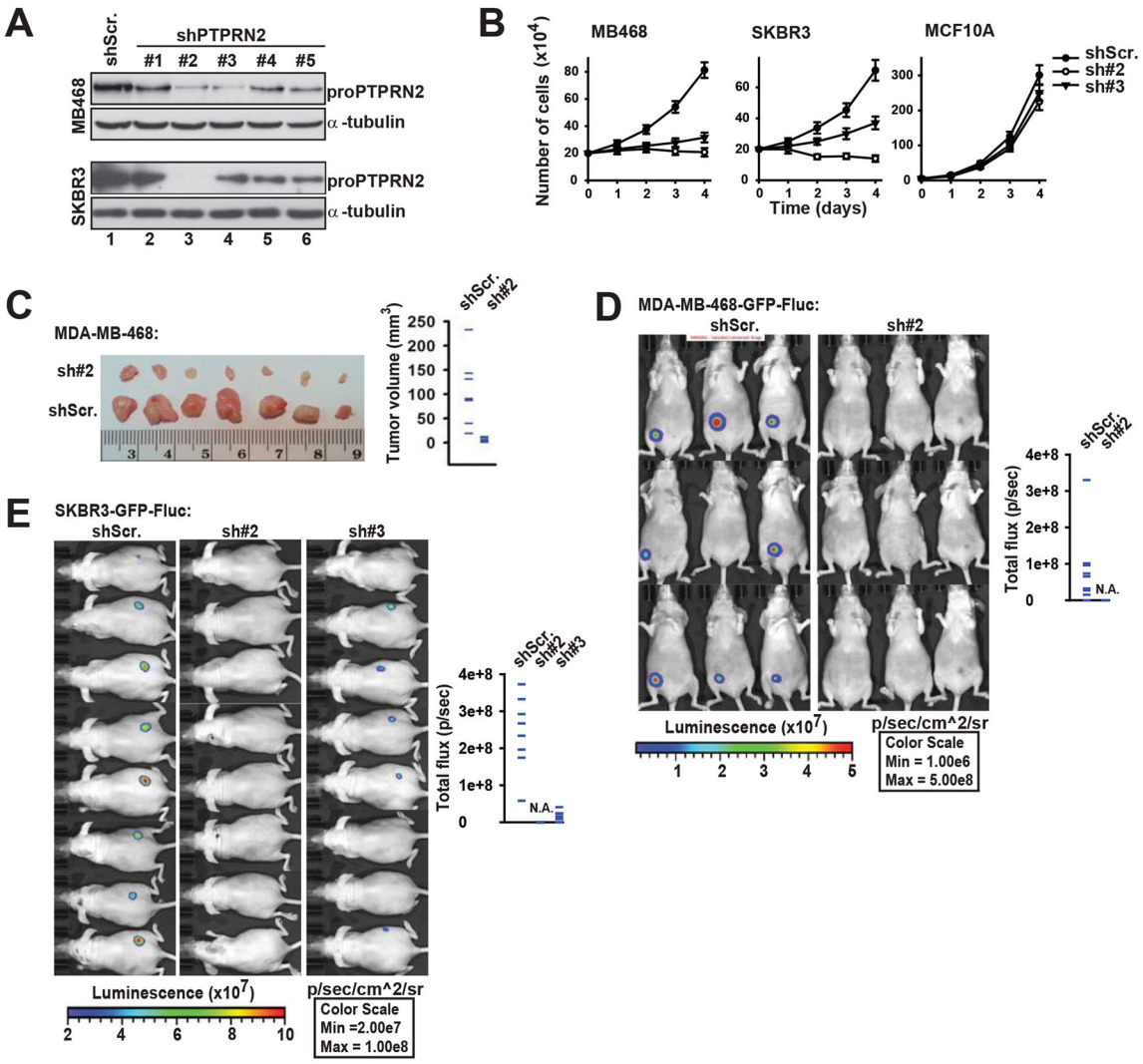

Figure 2. ProPTPRN2 knockdown suppresses cell proliferation and tumor growth

A, WB analysis of proPTPRN2 and α-tubulin in MDA-MB-468 (MB468) or SKBR3 cells stably expressing control (shScr.) or PTPRN2 shRNA (shPTPRN2). B, Growth curves of MDA-MB-468 or SKBR3 cells stably expressing shScr. or shPTPRN2 (sh#2 and sh#3). The representative growth curves from two independent experiments were shown (± s.e.m., n=3). C, Excised tumors and calculated volumes in nude mice injected with MDA-MB-468 cells bearing shPTPRN2 (sh#2) or shScr. at day 30 day after injection are shown (n=7 mice per group). D, Bioluminescence imaging of mouse mammary tumors after orthotopic injection of MDA-MB-468-GFP-Fluc cells bearing shPTPRN2 (sh#2) or shScr. at day 24 after injection (n=9 mice per group). Quantification of bioluminescence imaging signal intensity is presented to the right. E, Bioluminescence imaging of mice after subcutaneous injection of SKBR3-GFP-Fluc cells bearing shPTPRN2 (sh#2), shPTPRN2 (sh#3) or shScr. at day 24 after injection is shown (n=8 mice per group).

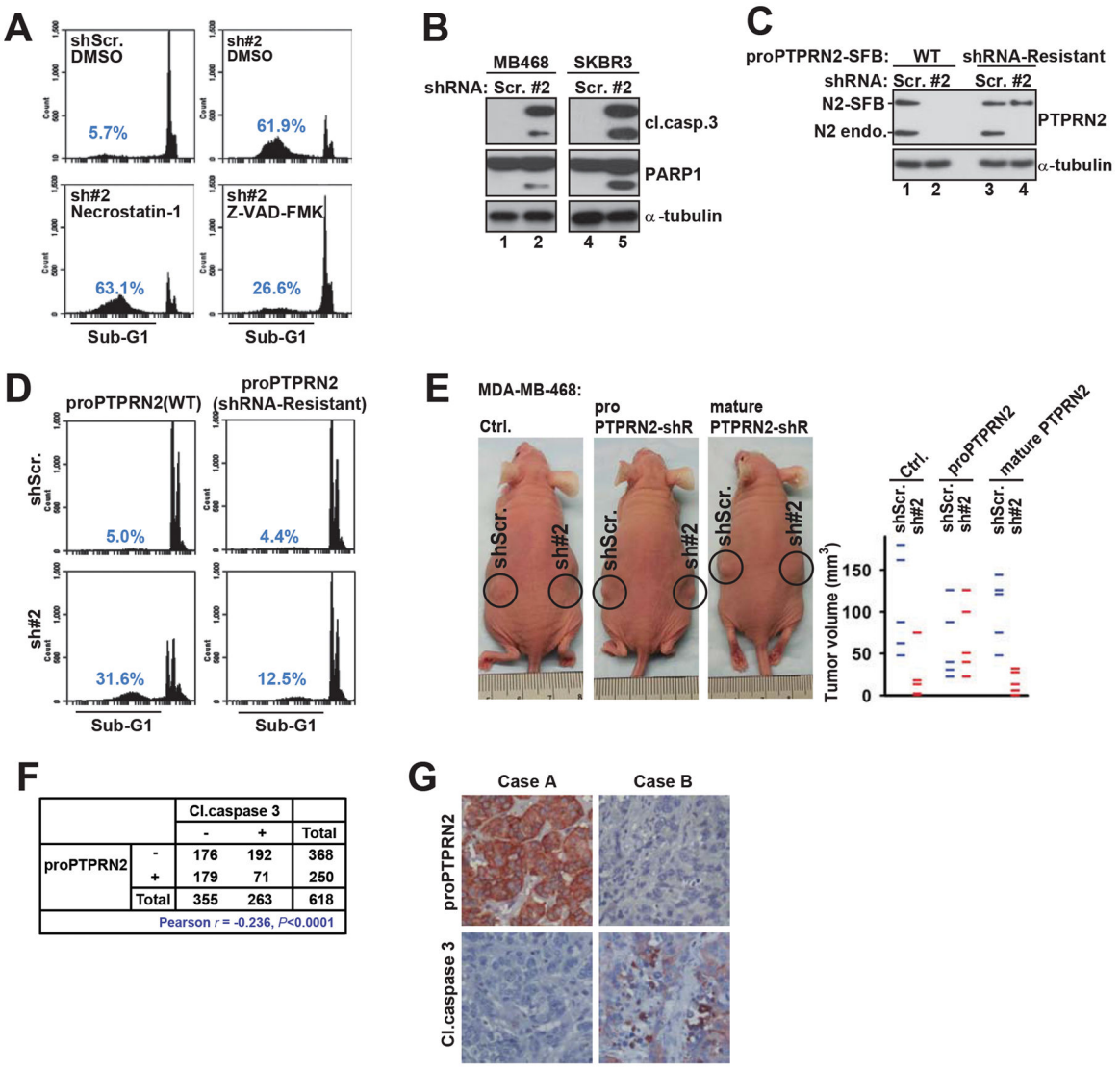

		Cl.caspase 3		
		-	+	Total
proPTPRN2	-	176	192	368
	+	179	71	250
	Total	355	263	618

Pearson r = -0.236, P<0.0001

Figure 3. ProPTPRN2 knockdown induces apoptosis

A, Cell cycle distribution of MDA-MB-468 cells stably expressing control (shScr.) or PTPRN2 shRNA (sh#2). Flow cytometry of cells treated with necrostatin-1 (30μM) or Z-VAD-FMK (30μM) for 3 days is shown. B, MDA-MB-468 (MB468) or SKBR3 cells stably expressing control (shScr.) or PTPRN2 shRNA (sh#2) were cultured for 3 days and analyzed by Western blotting using the indicated antibodies. (C and D) MDA-MB-468 cells stably expressing SFB-tagged wild-type proPTPRN2 (WT) or sh#2-resistant proPTPRN2, along with control (shScr.) or PTPRN2 shRNA (sh#2) were grown for 3 days and analyzed by flow cytometry (D), or Western blotting using the indicated antibodies (C). E, MDA-MB-468 cells stably expressing SFB-tagged sh#2-resistant proPTPRN2 (proPTPRN2-shR), mature PTPRN2 (mature PTPRN2-shR) or empty vector alone (Ctrl.) along with control (shScr.) or PTPRN2 shRNA (sh#2) were subcutaneously injected into nude mice. Tumor volumes were measured at day 24 after injection, (n=5 mice per group). F, Inverse correlation between proPTPRN2 and cleaved caspase 3 expression status (Pearson r =

−0.236, $P < 0.0001$). 618 cases NCI Prognostic TMAs were used for IHC with HPA026656 antibody. G, IHC staining of representative cases of breast carcinomas with high and low levels of proPTPRN2 and cleaved caspase 3. H-score system was used to quantify IHC results. For proPTPRN2 staining: $0 < \text{low} \leq 75$, $75 < \text{high} \leq 300$; for cleaved caspase 3 staining: $0 < \text{low} \leq 6$, $6 < \text{high} \leq 300$.

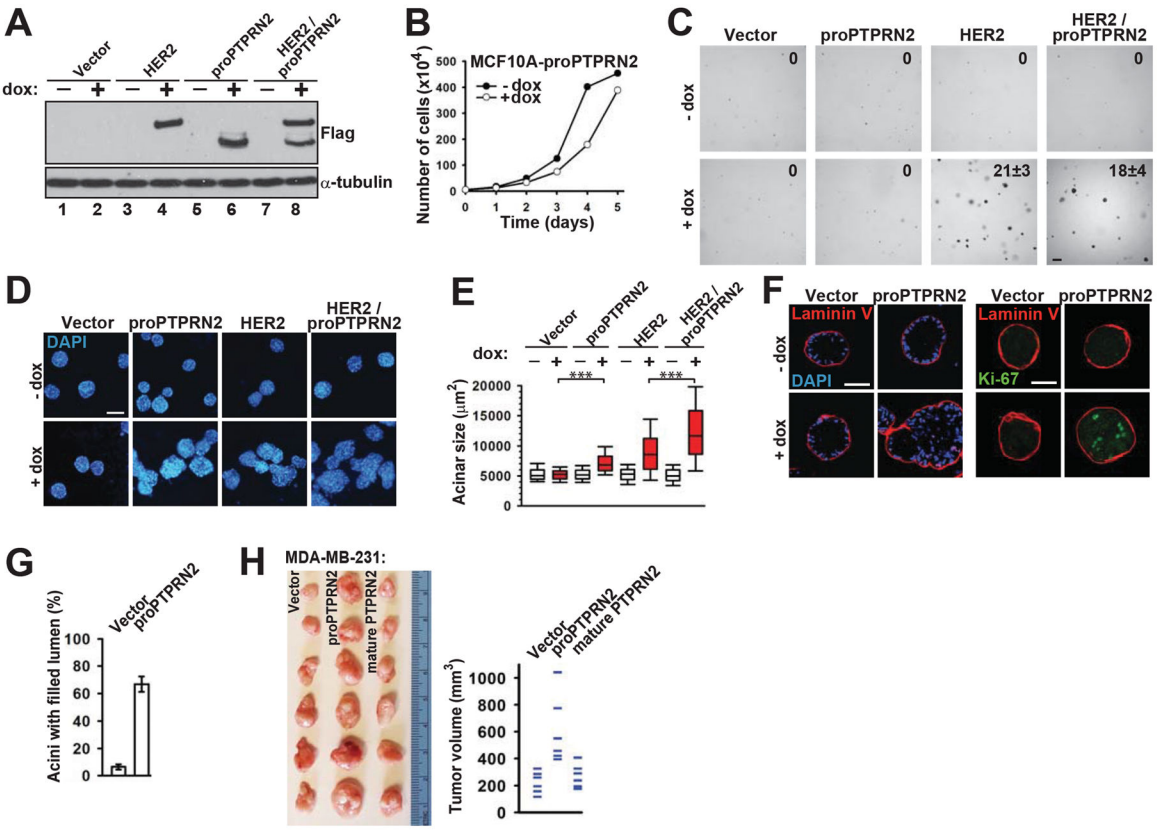

Figure 4. Ectopic expression of proPTPRN2 enhances tumor growth

A, MCF10A cells stably expressing SFB-tagged HER2, proPTPRN2, or both were grown in monolayer cultures with or without doxycycline (dox; 1 μg/ml) and analyzed by Western blotting using the indicated antibodies. B, Growth curves of MCF10A cell lines shown in (A). C, Soft agar colony formation of the indicated MCF10A cell lines in the presence or absence of doxycycline. Representative fields at day 30 day and the average number of colonies counted in 5 fields of view (±standard deviation) are shown. Scale bar, 200 μm. (D and E) Indicated MCF10A cell lines were grown in Matrigel in the presence or absence of doxycycline for 14 days and acinar structures were analyzed by DAPI staining (D). Scale bars, 100 μm. Acinar sizes shown in (E) were calculated from (D), n > 130 per group (***$P < 0.001$). (F and G) Acini formed by the indicated MCF10A cell lines were analyzed by confocal immunofluorescence using laminin V as a basal polarity marker as well as DAPI and proliferation marker Ki67, to analyze luminal filling (F). Scale bars, 50 μm. Percentage of acini with filled lumen (± s.e.m., n=50 per group) is shown in (G). H, MDA-MB-231 cells stably expressing SFB-tagged proPTPRN2 or mature PTPRN2, or vector alone were subcutaneously injected into nude mice and formed tumors were excised and measured at day 21 after injection (n=6 mice per group).

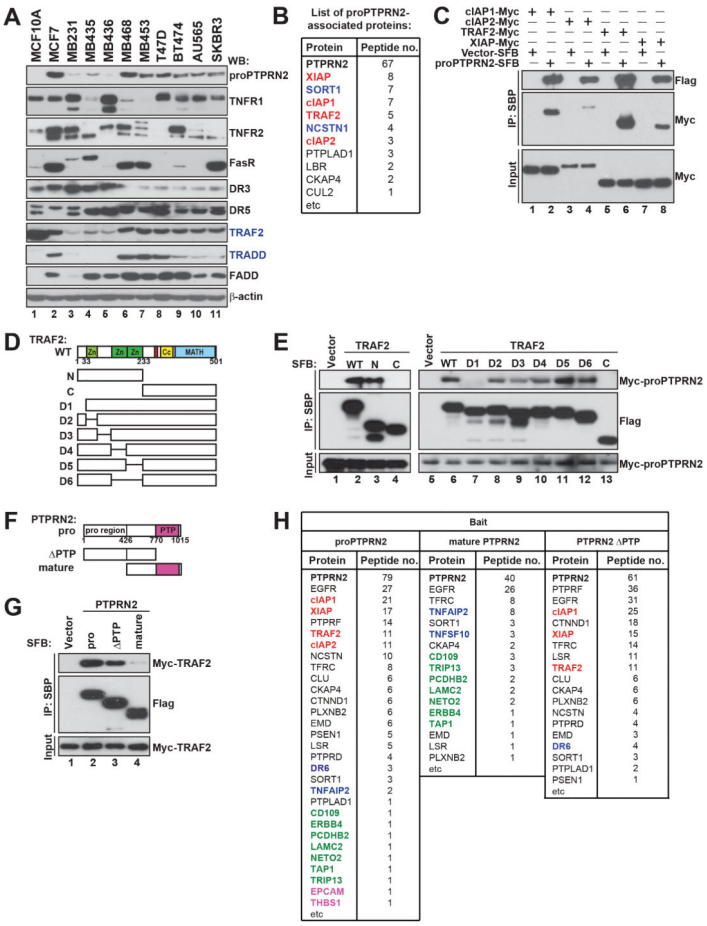

Figure 5. ProPTPRN2 but not the mature isoform of PTPRN2 interacts with the TRAF2 complex

A, Western blot (WB) analysis of normal and breast cancer cell lines examined for proPTPRN2, death receptors and components of the TRAF2 complex, as indicated. B, List of proteins co-immunoprecipitated with proPTPRN2 from HEK293T cells, as identified by mass spectrometry. C, Co-immunoprecipitation (Co-IP) of SFB-tagged proPTPRN2 with Myc-tagged cIAP1, cIAP2, XIAP, TRAF2 after transient co-expression in HEK293T cells. Proteins were co-IPed using streptavidin-binding peptide (SBP) beads and analyzed by WB with the indicated antibodies. Input and IP fractions are shown. D, Schematic diagram of TRAF2 proteins used in this study. E, Co-IP of SFB-tagged TRAF2 proteins with Myc-tagged proPTPRN2 after transient co-expression in HEK293T cells. Proteins were co-IPed using SBP beads and analyzed by WB with the indicated antibodies. Input and IP fractions are shown. F, Schematic diagram of PTPRN2 proteins used in this study. G, Co-IP of SFB-tagged PTPRN2 proteins with Myc-tagged TRAF2 after transient co-expression in HEK293T cells. Input and IP fractions were analyzed by WB using the indicated antibodies. H, List of proteins associated with the indicated PTPRN2 proteins, as identified by mass spectrometry. SFB-tagged proPTPRN2, mature PTPRN2 or proPTPRN2 lacking the PTP domain (ΔPTP) were stably expressed in MDA-MB-468 cells and co-immunoprecipitated using SBP beads. For the complete list and associated data, see Supplementary Table 1.

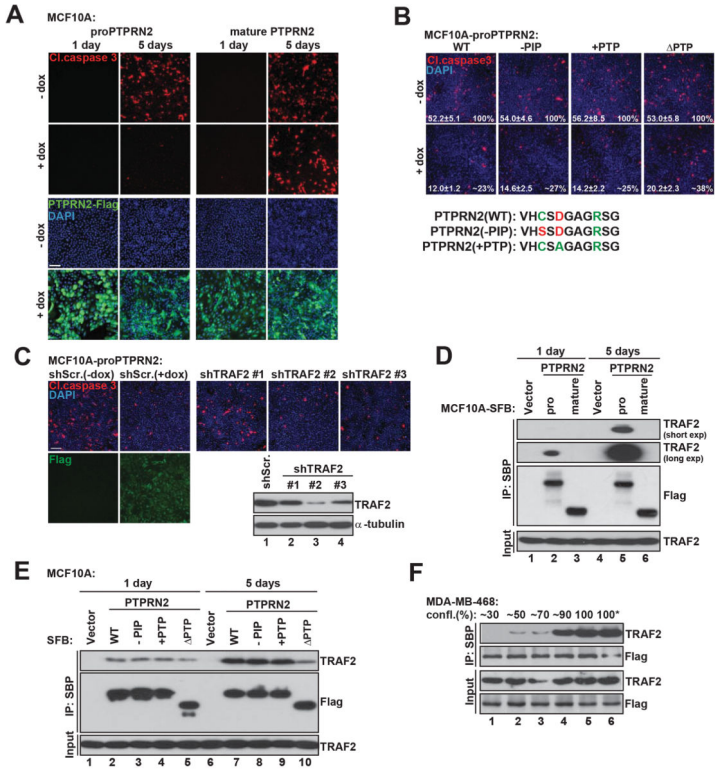

Figure 6. Ectopic expression of proPTPRN2 inhibits density-induced apoptosis in MCF10A cells

A, MCF10A cells stably expressing SFB-tagged proPTPRN2 or mature PTPRN2 were cultured at 100% confluence for 1 or 5 days in the presence or absence of doxycycline and monitored for caspase 3 cleavage using immunofluorescence microscopy. B, MCF10A cells stably expressing SFB-tagged proPTPRN2 (WT) or the mutant proteins with inactivated phosphoinositide phosphatase activity (−PIP) or with restored protein tyrosine phosphatase activity (+PTP), or lacking the PTP domain (ΔPTP) were cultured at 100% confluence for 5 days in the presence or absence of doxycycline and monitored for caspase 3 cleavage by immunofluorescence microscopy. Data shown are the average number of cleaved caspase 3-positive cells counted in 5 fields of view (± s.e.m). C, MCF10A cells stably expressing SFB-tagged proPTPRN2 were co-transfected with control (shScr.) or TRAF2 (sh#1, sh#2, sh#3) shRNAs and cultured at 100% confluence for 5 days in the presence or absence of doxycycline. Immunofluorescence microscopy was done using cleaved caspase 3 and Flag (to detect proPTPRN2) antibodies. Insert shows WB with TRAF2 antibody to confirm its knockdown. D, MCF10A cells stably expressing empty vector or SFB-tagged proPTPRN2 (pro) or mature PTPRN2 were cultured at 100% confluence for 1 or 5 days in the presence or absence of doxycycline. Proteins were co-immunoprecipitated using SBP beads and analyzed by WB with the indicated antibodies. Input and IP fractions are shown. E, MCF10A cells stably expressing empty vector or SFB-tagged proPTPRN2 (WT) or the corresponding mutant proteins as in (B) were cultured at 100% confluence for 1 or 5 days in the presence or absence of doxycycline. Proteins were co-immunoprecipitated using SBP beads and analyzed by WB with the indicated antibodies. Input and IP fractions are shown. F, MDA-MB-468 cells stably expressing SFB-tagged proPTPRN2 were cultured to various confluences, as indicated, and used for co-IP experiments. Star indicates cells that were

cultured at 100% confluence for 2 days. Proteins were co-IPed using SBP beads and analyzed by WB with the indicated antibodies. Input and IP fractions are shown.

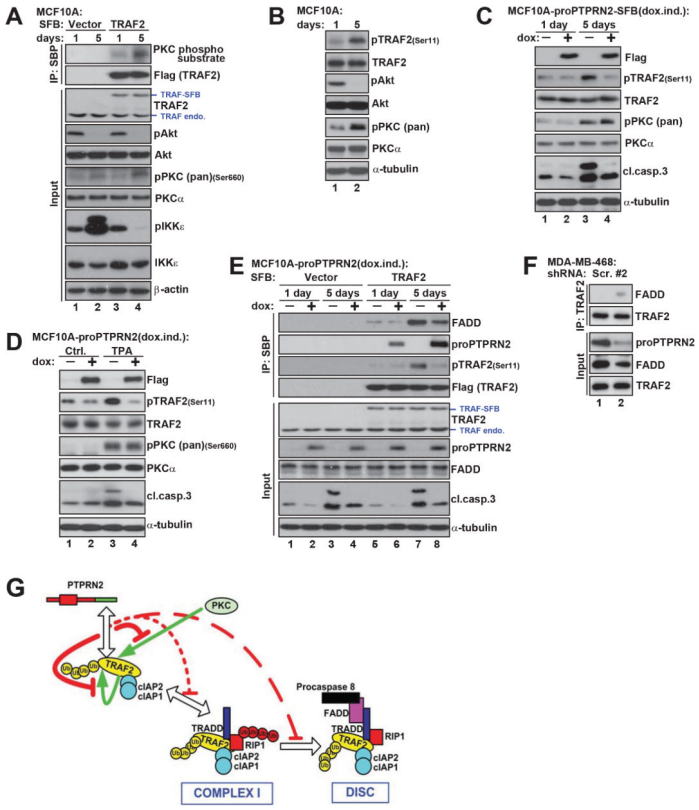

Figure 7. Binding of proPTPRN2 suppresses TRAF2 phosphorylation by PKC kinase and its complex formation with FADD

A, Co-immunoprecipitation (co-IP) and Western blot (WB) analysis of MCF10A cells stably transfected with empty vector (Vector) or SFB-tagged TRAF2, cultivated at 100% confluence for 1 or 5 days with doxycycline (1 μg/ml). SBP, streptavidin-binding peptide. B, WB analysis of MCF10A cells stably transfected with SFB-tagged TRAF2, cultivated at 100% confluence for 1 or 5 days with doxycycline (1 μg/ml). C, WB analysis of MCF10A cells stably transfected with SFB-tagged proPTPRN2, placed under the control of doxycycline-inducible promoter and cultivated at 100% confluence for 1 or 5 days with or without doxycycline (dox; 1 μg/ml) in medium. D, WB analysis of MCF10A cells stably transfected with SFB-tagged proPTPRN2, placed under the control of doxycycline-inducible promoter and cultivated at 100% confluence for 1 day with or without doxycycline (dox; 1 μg/ml) in medium and treated with cycloheximide (20 μg/ml) (Ctrl.), or with cycloheximide (20 μg/ml) and 12-O-Tetradecanoylphorbol-13-acetate (0.8 μg/ml) (TPA) for 3h (TPA). E, Co-IP and WB analysis of MCF10A cells stably transfected with empty vector (Vector) or SFB-tagged TRAF2 together with proPTPRN2, placed under the control of doxycycline-inducible promoter and cultivated at 100% confluence for 1 or 5 days with or without dox (1 μg/ml) in medium. F, Co-IP and WB analysis of MDA-MB-468 cells expressing control shRNA (shScr.) or PTPRN2 shRNA (sh#2). G, A model of how proPTPRN2 may be involved in inhibition of apoptosis.